AFRL-PR-WP-TP-2006-231

ISLAND GROWTH OF Y_2BaCuO_5 NANOPARTICLES IN $(211_{\sim 1.5\ nm}/123_{\sim 10\ nm})xN$ COMPOSITE MULTILAYER STRUCTURES TO ENHANCE FLUX PINNING OF $YBa_2Cu_3O_{7-\delta}$ FILMS

T. Haugan, P.N. Barnes, I. Maartense, C.B. Cobb, E.J. Lee, and M. Sumption

MARCH 2003

Approved for public release; distribution is unlimited.

STINFO COPY

PROPULSION DIRECTORATE
AIR FORCE MATERIEL COMMAND
AIR FORCE RESEARCH LABORATORY
WRIGHT-PATTERSON AIR FORCE BASE, OH 45433-7251

REPORT DOCUMENTATION PAGE

Form Approved
OMB No. 0704-0188

1. REPORT DATE *(DD-MM-YY)*	2. REPORT TYPE	3. DATES COVERED *(From - To)*
March 2003	Journal Article Postprint	

4. TITLE AND SUBTITLE

ISLAND GROWTH OF Y_2BaCuO_5 NANOPARTICLES IN $(211_{\sim 1.5\ nm}/123_{\sim 10\ nm})xN$ COMPOSITE MULTILAYER STRUCTURES TO ENHANCE FLUX PINNING OF $YBa_2Cu_3O_{7-\delta}$ FILMS

5a. CONTRACT NUMBER
In-house

5b. GRANT NUMBER

5c. PROGRAM ELEMENT NUMBER
61102F/62203F

6. AUTHOR(S)

T. Haugan, P.N. Barnes, I. Maartense, and C.B. Cobb (AFRL/PRPG)
E.J. Lee and M. Sumption (The Ohio State University)

5d. PROJECT NUMBER
3145

5e. TASK NUMBER
32

5f. WORK UNIT NUMBER
31453Z9

7. PERFORMING ORGANIZATION NAME(S) AND ADDRESS(ES)

Power Generation Branch (AFRL/PRPG)
Power Division
Propulsion Directorate
Air Force Research Laboratory, Air Force Materiel Command
Wright-Patterson Air Force Base, OH 45433-7251

The Ohio State University
Department of Materials Science and Engineering
Columbus, OH 43210

8. PERFORMING ORGANIZATION REPORT NUMBER
AFRL-PR-WP-TP-2006-231

9. SPONSORING/MONITORING AGENCY NAME(S) AND ADDRESS(ES)

Propulsion Directorate
Air Force Research Laboratory
Air Force Materiel Command
Wright-Patterson AFB, OH 45433-7251

10. SPONSORING/MONITORING AGENCY ACRONYM(S)
AFRL-PR-WP

11. SPONSORING/MONITORING AGENCY REPORT NUMBER(S)
AFRL-PR-WP-TP-2006-231

12. DISTRIBUTION/AVAILABILITY STATEMENT
Approved for public release; distribution is unlimited.

13. SUPPLEMENTARY NOTES

Journal article postprint published in the Journal of Materials Research, Vol. 18, No. 11, Nov. 2003, published by the Materials Research Society. PAO case number: ASC 03-1147; Date cleared: 05 May 2003.

14. ABSTRACT

A controlled introduction of second-phase Y_2BaCuO_5 (211) nanoparticles into $YBa_2Cu_3O_{7-\delta}$ (123) thin films was achieved for the first time for the purpose of increasing flux pinning. The island-growth mode of 211 on 123 was utilized to obtain an area particle density $>10^{11}$ cm^{-2} of 211 thick-disk-shaped nanoparticles in individual layers. Composite layered structures of $(211_y$ nanoparticles/$123_z)\times N$ were deposited by pulsed laser deposition on $LaAlO_3$ substrates, with N bilayers = 24 to 100, y thickness = 1 to 2 nm, and z thickness = 6 to 15 nm (assuming continuous layer coverage). With 211 addition, the critical current densities at 77 K were higher at magnetic fields as low as 0.1 T and increased as much as approximately 300% at 1.5 T. The superconducting transition temperature was reduced by approximately 2 to 4 K for 211 volume fraction <20%. Reinitiation of 123 growth after every 211 layer resulted in a smooth and flat surface finish on the films and also greatly reduced surface particulate formation especially in thicker films (~1 μm).

15. SUBJECT TERMS island growth of YBCO, flux pinning, superconducting

16. SECURITY CLASSIFICATION OF:			17. LIMITATION OF ABSTRACT:	18. NUMBER OF PAGES	19a. NAME OF RESPONSIBLE PERSON (Monitor)
a. REPORT	b. ABSTRACT	c. THIS PAGE			Paul N. Barnes
Unclassified	Unclassified	Unclassified	SAR	12	19b. TELEPHONE NUMBER *(Include Area Code)* N/A

Island growth of Y_2BaCuO_5 nanoparticles in $(211_{\sim 1.5\ nm}/123_{\sim 10\ nm})\times N$ composite multilayer structures to enhance flux pinning of $YBa_2Cu_3O_{7-\delta}$ films

T. Haugan,[a] P.N. Barnes, I. Maartense, and C.B. Cobb
Air Force Research Laboratory, Wright-Patterson Air Force Base, Ohio 45433-7919
E.J. Lee and M. Sumption
Department of Materials Science and Engineering, The Ohio State University, Columbus, Ohio 43210

(Received 26 March 2003; accepted 1 August 2003)

A controlled introduction of second-phase Y_2BaCuO_5 (211) nanoparticles into $YBa_2Cu_3O_{7-\delta}$ (123) thin films was achieved for the first time for the purpose of increasing flux pinning. The island-growth mode of 211 on 123 was utilized to obtain an area particle density $>10^{11}$ cm^{-2} of 211 thick-disk-shaped nanoparticles in individual layers. Composite layered structures of $(211_y$ nanoparticles/$123_z)\times N$ were deposited by pulsed laser deposition on $LaAlO_3$ substrates, with N bilayers = 24 to 100, y thickness = 1 to 2 nm, and z thickness = 6 to 15 nm (assuming continuous layer coverage). With 211 addition, the critical current densities at 77 K were higher at magnetic fields as low as 0.1 T and increased as much as approximately 300% at 1.5 T. The superconducting transition temperature was reduced by approximately 2 to 4 K for 211 volume fraction <20%. Reinitiation of 123 growth after every 211 layer resulted in a smooth and flat surface finish on the films and also greatly reduced surface particulate formation especially in thicker films (~1 μm).

I. INTRODUCTION

The development of coated conductor wire technologies for biaxially aligning $YBa_2Cu_3O_{7-\delta}$ (123) on buffered metallic substrates with $J_c > 1$ MA/cm^2 offers great promise for incorporating YBCO coated conductors in applications such as alternating current (ac) wires, generators, or motors operating at 77 K.[1–7] $YBa_2Cu_3O_{7-\delta}$ has excellent properties at 77 K for such applications including high critical current densities (J_c) due to good flux pinning in applied magnetic fields, which is critical for most applications.[1,2] Typically for magnetic fields applied in the worst orientation B_{appl} // c axis, J_c will decrease by a factor of 10 to 100 for B_{appl} = 1 T to 5 T, respectively.[8,9] It is of interest to increase J_c even further, as such improvements will not only lower overall system costs for applications, but allow for reductions in the weight and size of the system. For applications such as high-field magnets, the value of $J_c(H)$ places an upper limit on the magnetic field that can be produced for a given coil design.

Because $YBa_2Cu_3O_{7-\delta}$ is a type-II superconductor, it is understood that to increase flux pinning, a high density of nonsuperconducting defects must be added to the material.[2–4] Assuming each defect can pin one fluxon $\Phi_o = 2.07 \times 10^{-11}$ T·cm^2, the area particle density required to pin a magnetic field of strength M (Tesla) would need to be of the order ~$(M/2) \times 10^{11}$ cm^{-2} (Ref. 3). An area particle density of second-phase defects $>10^{11}$ cm^{-2} was previously achieved in low-temperature NbTi superconductors to increase J_c;[4] however, to our knowledge an area particle density of second-phase (rather than intrinsic) defects $>10^{10}$ cm^{-2} has not been achieved yet for 123. An additional requirement for effective pinning defects is that the size must be approximately the same size or greater than the coherence length of the materials, which for 123 is approximately 2 nm at 4.2 K and approximately 4 nm at 77 K.[2,10]

In this work, Y_2BaCuO_5 (211) nanosize particles were incorporated directly into the 123 matrix to increase the flux pinning. Y_2BaCuO_5 as a pinning agent has several advantages. From phase equilibria studies, 211 coexists in stable chemical equilibrium with 123 at 850–900 °C and in varying partial O_2 pressure atmospheres.[11] The requirement for chemical stability is arguably greater for

[a]Address all correspondence to this author.
e-mail: timothy.haugan@wpafb.af.mil

nanosize materials, as chemical reactions occur faster on this size scale which can degrade the superconductor,[12] which might otherwise procede slowly in bulk reactions. Y_2BaCuO_5 also has an additional advantage for pulsed laser deposition (PLD), as it was possible to use the same deposition parameters for 211 as for high-quality 123; that is, the same O_2 pressures and laser fluences were used, which reduced the processing time and simplified the deposition. Finally, 211 has an advantage to achieve island growth of particles, as it has a relatively large lattice mismatch with 123 of 2% to 8% for different combinations of crystalline orientations. Thin film growth on lattice-mismatched substrates generally occurs via the island growth method, as film growth is energetically favored (preferred) to grow on the lattice-matched island-nucleated phase rather than on the lattice-mismatched substrate.[13,14] Therefore, it was not unexpected that 211 was observed to grow as island-growth clusters in this work with high area particle density $>10^{11}$cm^{-2} and provided a near-optimal size and number of pinning defects.

A large base of knowledge exists in the literature regarding addition of 211 to 123 in bulk or melt-processed materials to improve flux pinning (Refs. 3, 15–20 and references therein); however, there has been no attempt thus far to incorporate 211 particles directly into the microstructure of 123 thin films. While some studies with bulk materials showed improvement of flux pinning with 211 addition,[15,17–20] other studies reported otherwise possibly because of large 211 particle size.[16] In fully processed bulk materials, the 211 particle size is usually submicrometer to micrometer and the area particle density is typically very low, $<10^{10}$ cm^{-2}, although a very few 10–100-nm size particles can exist with area particle density $<10^{10}$ cm^{-2} (Refs. 17–20). This area particle density is too small to cause directly a large increase of flux pinning; therefore, to explain an increase it was suggested that networks of dislocation defects surrounding the 211 particles with high number density could act as pinning centers.[3,18–20] In the work herein, the size of 211 incorporated into 123 is on the order 10–15 nm, and the surface number density is sufficiently high to cause an increase of flux pinning without the possible effect of dislocations.

The structures studied in this paper were alternating depositions of 211 nanoparticle layers and 123 thin films multiple times, referred to herein as $(211/123)\times N$. When conceptualized in three dimensions, this structure contains 211 defects spaced about 6–20-nm apart in directions both parallel and perpendicular to the *c* axis of the film, depending on the 123 layer thickness chosen and the 211 island-growth conditions. While the 211 pinning arrangement is not symmetrically uniform, the layering approach does appear to achieve a near-uniform dispersion of 211 particles.

II. EXPERIMENTAL

Multiple layers of 123 and 211 nanoparticles were deposited by pulsed laser deposition, using parameters and conditions optimized previously for 123.[21,22] The laser ablation targets were purchased commercially (Superconductive Components Inc., Columbus, OH). The 123 target was 92% dense and was made using powder processed by chemical precipitation (nominally 99.999% pure); the 211 target was 87% to 88% dense and was made with solid-state powders (99.9% purity). The depositions were automated and controlled by computer program, with the laser pulses trigger-actuated by computer control. Film growth was stopped between each layer for a period of about 13 s, when the other target was rotated into position. For multilayer sample $(211_{1.6\ nm}/123_{6.2\ nm})\times 35$, film growth was performed by manually switching targets during which the film growth was stopped for an average period of about 80 s. An excimer laser (Lambda Physik USA Inc., model LPX 305i, Ft. Lauderdale, FL) operating at 248 nm was used. The laser fluence was approximately 3.2 J/cm^2 and the ablation spot size was approximately 1×6.5 mm^2. The laser pulse rate was 4 Hz. The target-to-substrate distance was 6 cm. The oxygen deposition pressure was 300 mtorr for both 211 and 123 phases, as measured with capacitance manometer and convectron gauges within <10% variation. Oxygen gas (99.999% purity) flowed into the chamber during growth at approximately 1 l/min, and the oxygen pressure in the chamber was kept constant in the chamber using a downstream throttle-valve control on the pumping line. The targets were resurfaced periodically with sandpaper and were conditioned prior to any film deposition with ~80 shots/site using a similar laser fluence of 2–4 J/cm^2. The targets were rotated and rastered up and down, which improved the uniformity of target wear. The laser beam was scanned across 1.2 cm of the 2.5-cm-diameter targets to improve the film thickness uniformity in the deposition zone. The plume varied only slightly as a consequence of scanning. The $LaAlO_3$ (100) and $SrTiO_3$ (100) single crystal substrates were ultrasonically cleaned for 2 min each using first acetone, followed by dehydrated ethyl alcohol or isopropyl alcohol. Crystal substrates were provided by the manufacturer epitaxially polished on both sides ($LaAlO_3$) and on one side ($SrTiO_3$), and were attached to the heater using a thin layer of colloidal Ag paint. Substrates sizes were 3.2×3.2 mm^2 for magnetic J_c measurements and 3×12 mm^2 for transport J_c measurements.

The background pressure in the chamber was reduced to $<10^{-6}$ torr prior to depositions. Samples were heated from room temperature to deposition temperature of 785 °C at 1270 °C/h. After deposition, films were cooled from 785 °C to 750 °C at 1270 °C/h before turning off the vacuum pumps and O_2 pressure control. Subsequently, the O_2 flow was increased to approximately 1.5 l/min into the chamber. The films were then cooled

from 750 °C to 500 °C at a rate of 1270 °C/h and were held at 500 °C for 30 min, during which the O_2 pressure reached 1 atm. The films were cooled from 500 °C to 250 °C at about 1250 °C/h and from 250 °C to room temperature using the natural cooling rate of the heater block (~800 °C/h).

The 123 layer and 211 "pseudo" layer thickness was closely estimated by calibrating the deposition rates of both 123 and 211 for many deposition runs both before and after multilayer depositions. Although the 211 layer contains discontinuous nanoparticles, a 211 "pseudo" layer thickness is referred to in this paper which is calculated assuming a smooth continuous layer. For similar conditions, 211 was observed to deposit on $Zr(Y)O_2$ or $LaAlO_3$ substrates at a slightly higher rate, with the ratio of deposition rates (211/123) = 1.26 ± 0.09. After measuring the total film thickness of the composite structure film, this ratio together with the number of pulses was used to determine the relative 123 and 211 pseudo layer thickness achieved for each composite film. While the sticking coefficient of the initial 211 or 123 layers may not be the same as for bulk material, this value provides an estimate for the relative layer thickness of the (211 nanoparticle/123)×*N* structures.

After deposition, current and voltage contacts for J_c measurements were patterned onto the films by dc magnetron sputter deposition of Ag with ~3 μm thickness. The resistance of the Ag-123 contacts was reduced by annealing in pure O_2 at 550 °C for 30 min, followed by annealing at 500 °C for 0.5–2 h, with heating and cooling rates of 200 °C/h.[23] Critical currents were measured over macrobridges 0.3-cm long and 0.05-cm wide, patterned using 248-nm KrF laser etching through a precisely machined Al_2O_3 mask or using standard chemical resist lithographic methods. The film thickness of every sample was measured multiple times across acid-etched steps next to or directly across bridges with a P-15 Tencor profilometer (KLA Tencor, Milpitas, CA), and with scanning electron microscopy (SEM) cross sections. Care was used to measure with the profilometer only in twin-free areas of the $LaAlO_3$ substrates, which were observed visually at high magnification.

Transport critical current density (J_c) measurements were made in liquid nitrogen at 77.2 K with the 4-probe probe method (self-field) using pogo pins for current contacts[24] and a 1 μv/cm criterion. Systems to measure temperature and critical current were calibrated on a regular basis. Current was applied to the sample by a step-ramp method: a current step interval of 0.2 to 0.5 s, a ramp rate of 0.25 to 1.0 A/s, and a voltage sample period 2 to 4 times smaller than the current step interval. The maximum current step size was 0.2 A. Measurements of J_c were repeatable for these ranges of step-ramp parameters. Current sources and voltmeters for measurements were calibrated on a regular basis.

The superconducting transition temperature (T_c) was measured using an ac susceptibility technique with the amplitude of the magnetic sensing field, *h*, varied from 0.025 Oe to 2.2 Oe at a frequency of approximately 4 kHz.[25,26] Note that the ac susceptibility technique provides information about primary and secondary transitions of the entire film, rather than a defined path that is obtained with transport T_c measurements. T_cs were measured immediately after film deposition and prior to adding Ag contacts. Samples were mounted onto the end of a sapphire rod and measured as the samples were warmed through the transition region at very slow rate of approximately 0.06 K/min. The T_c measurements were accurate within ≤0.1 K at three calibration points: liquid He at 4.2 K, liquid N_2 at 77.2 K, and room temperature.

X-ray diffraction θ–2θ scans were made with a Rigaku diffractometer (Rigaku International Corporation, Tokyo, Japan) with a 2θ step-size of 0.03 Å and a count time of 1.8 s. Magnetic J_c measurements were made with a vibrating sample magnetometer (VSM) in fields of 0 to 1.6 T and a ramp rate from 9000 (A/m·s) to 42,000 (A/m·s). The J_c of the square samples was estimated using a simplified Bean model $J_c = 15\Delta M/R$, where *M* is magnetization/volume from *M–H* loops and *R* is the radius of volume interaction = square side for consistency.[27] The film thickness and dimensions of each sample were measured multiple times to reduce errors of superconducting volume and *R* to <5%.

III. RESULTS AND DISCUSSION

The orientation and type of phases present in the films were studied by x-ray diffraction (XRD), as shown in Fig. 1 for a multilayer film compared to reference 211 and 123 films. For multilayer films, formation of the 211 phase was verified with XRD peaks for the a00, 0b0, 141, and 320 reflections observed with good intensity. However, peaks for the 131, 151, 222, and 260 reflections were missing, which suggests the 211 phase

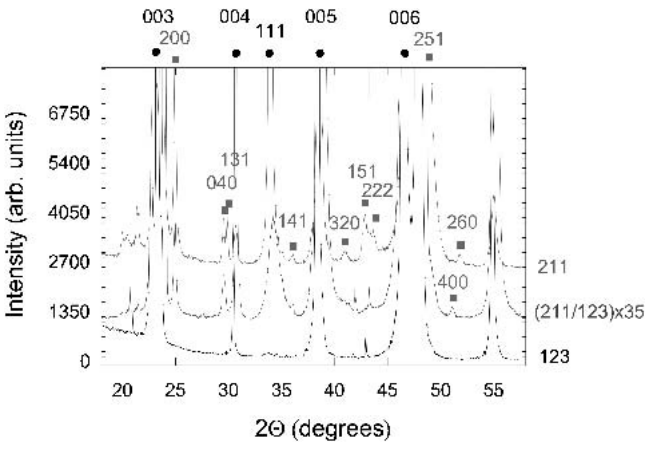

FIG. 1. Typical XRD θ–2θ scans of 211, $(211_{1.6\ nm}/123_{6.5\ nm})\times 35$, and 123 films deposited on $LaAlO_3$ substrates with 211 (■) and 123 (●) peaks labeled.

was growing with preferred orientations. Growth of 211 with a00 or 0b0 orientations on 123 might be expected, as the lattice mismatch is lower for this orientation (2% to 5%) than for other orientations (e.g., 5% to 8% lattice mismatch for 00c orientation growth).

The microstructures of a (211/123)×35 multilayer film were analyzed by planar-view transmission electron microscopy (TEM) as given in Fig. 2, where the round nature of second-phase particles can be seen that have Moiré fringelike patterns. The average size of a distribution of round particles in Fig. 2 was about 15 nm. Using this average particle size and assuming a diameter-to-height aspect ratio of approximately 4 observed with cross-sectional TEM, the 211 area particle density could be calculated from mass balance as approximately 2.4×10^{11} cm^{-2}, which is sufficient in theory to pin a 5-T field. However, this particle density should only be considered an initial estimate, as only one area of the film was examined and only large particles easily distinguishable were measured. With a smaller average particle size, the area density of particles would increase. Because the TEM sample area observed was not prepared or thinned uniformly, it was not possible to determine the distribution uniformity of the particles in Fig. 2.

To clarify, the composite structure of the samples is essentially a layered structure composed of "pure" 123 layers interleaved with layers that have 211 nanoparticles imbedded in a 123 matrix. The surface in question for the area particle density is for the various 211 layers distributed throughout the (211/123)×N composite structure. The spacing and distribution of nanoparticles as shown in Fig. 2 is sufficient to allow effective pinning on those sites, and an increase of $J_c(H)$ is expected.

The T_c transitions of a typical multilayer sample are shown in Fig. 3 compared to a reference 123 film. A T_c of approximately 89 K was consistently measured for

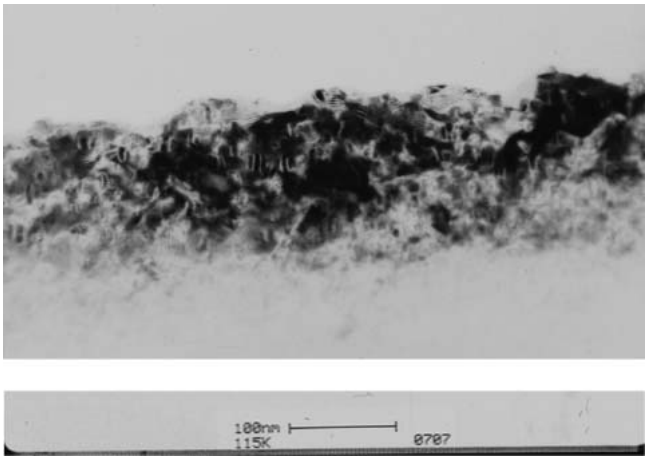

FIG. 2. TEM micrograph of a $(211_{\sim 1.6\ nm}/123_{\sim 6.5\ nm})\times 35$ multilayer film looking through the film surface (planar view). Spherical-shaped particles with fringelike patterns indicate second-phase material inside a primary phase matrix.

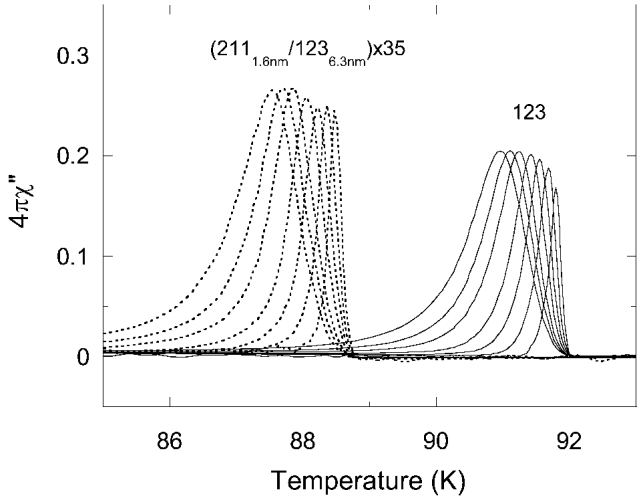

FIG. 3. T_c transitions by ac susceptibility of a $(211_{\sim 1.6\ nm}/123_{\sim 6.3\ nm})\times 35$ multilayer film compared to a 123 single-layer film with similar thickness. T_cs were measured with 0.025 Oe, 0.1 Oe, 0.25 Oe, 0.5 Oe, 1.0 Oe, 1.5 Oe, and 2.2 Oe applied fields, which broaden and move the transition to lower T_cs with higher applied magnetic fields.

this type of sample, which was reduced slightly from the T_c of a pure 123 sample of approximately 92 K. The reason for the decrease of T_c is unknown; however, one possible contribution to the decrease is that the 123 phase was compressively strained in the composite film because of the lattice mismatch with 211. A shift of the 00l peaks toward higher 2θ values was in general observed by XRD diffraction in Fig. 1, which suggests the 123 phase is under compressive strain along the c axis. Another possible contribution of the decrease of T_c is that the superconducting order parameter was suppressed, similar to the decrease of T_c observed in ion irradiation experiments that created amorphized regions.[28]

The J_cs of the (211/123)×N composite samples are shown in Fig. 4 at 77 K and are compared to a reference 123 film made using the same deposition conditions as well as to $J_c(H)$ plots for 123 films on single crystal or biaxially textured Ni substrates from the literature. In Fig. 4, the J_c of the (211/123)×N composite films showed significantly different pinning behavior in fields as low as 0.1 T when compared to all reference 123 single-layer tapes. At a higher field of 1.5 T an increase of J_c >300% was achieved, and the trend of the plots suggest that an even larger increase could be obtained for even higher field strengths. At zero applied field, the J_cs of the (211/123)×N composites tapes were on the order 2–3 MA/cm^2 at 77 K as determined by magnetic measurements in Fig. 4.

The transport J_cs of (211/123)×N composite samples were measured as well at 77.2 K in self-field. The transport J_cs were typically in the range 2–3 MA/cm^2 as measured for many samples, consistent with the range of J_cs measured by magnetization.

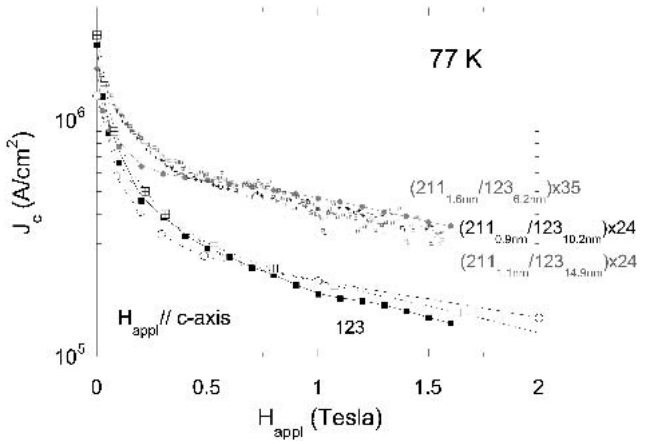

FIG. 4. J_c at 77 K as a function of applied magnetic field for multilayer films $(211_{1.6\ nm}/123_{6.2\ nm})\times35$ (●), $(211_{0.9\ nm}/123_{10.2\ nm})\times24$ (x), and $(211_{1.1\ nm}/123_{14.9\ nm})\times24$ (+), compared to 123 films grown in-house on $LaAlO_3$ (■), 123 on $LaAlO_3$ at 75 K (⊞),[8] and 123 on CeO_2/YSZ/Gd_2O_3/RABITS (Ni,W,Fe) substrates (⊙).[9] J_c was calculated using the entire film thickness including 211 and 123 layers.

In addition to improved magnetic properties, the films also showed unusually smooth surfaces with reduced particulate densities, especially for ~1-μm film thickness, as shown in Fig. 5. The multilayer films are highly dense and the film surfaces quite smooth at high magnification. It is believed that both increased film planarization and reduced particulate formation resulted from reinitiation of the 123 layer after the 211 layer, similar to the mechanism for growth of $(CeO_{2\sim0.2\ \mu m}/123)$ multilayers previously described.[29]

IV. CONCLUSIONS

Second-phase Y_2BaCuO_5 (211) nanosize particles were dispersed by layering into $YBa_2Cu_3O_{7-\delta}$ (123) thin films it is believed for the first time, utilizing the island-growth mechanism expected from thin-film growth of two lattice-mismatched materials. An area particle density estimated as $>10^{11}$cm^{-2} of 211 particles with size approximately 10–15 nm in diameter was achieved in individual layers of the composite structures with architecture $(211/123)\times N$ and N up to 100. This is the first time a second-phase area particle density $>10^{10}$ cm^{-2} has been obtained in 123 processed by any method. With addition of 211 particles, the critical current densities increased 300% for magnetic fields of 1.5 T at 77 K. The 123 phase grew with excellent *c*-axis orientation, and the 211 particles grew with preferred a00 or 0b0 and other orientations. The superconducting transition temperature reduced slightly to approximately 88–90 K from ~92 K with 211 volume fraction <20%. Reinitiation of 123 after every 211 layer resulted in a smooth and flat surface finish on the films and also greatly reduced surface particulate formation especially in thicker films (~1 μm).

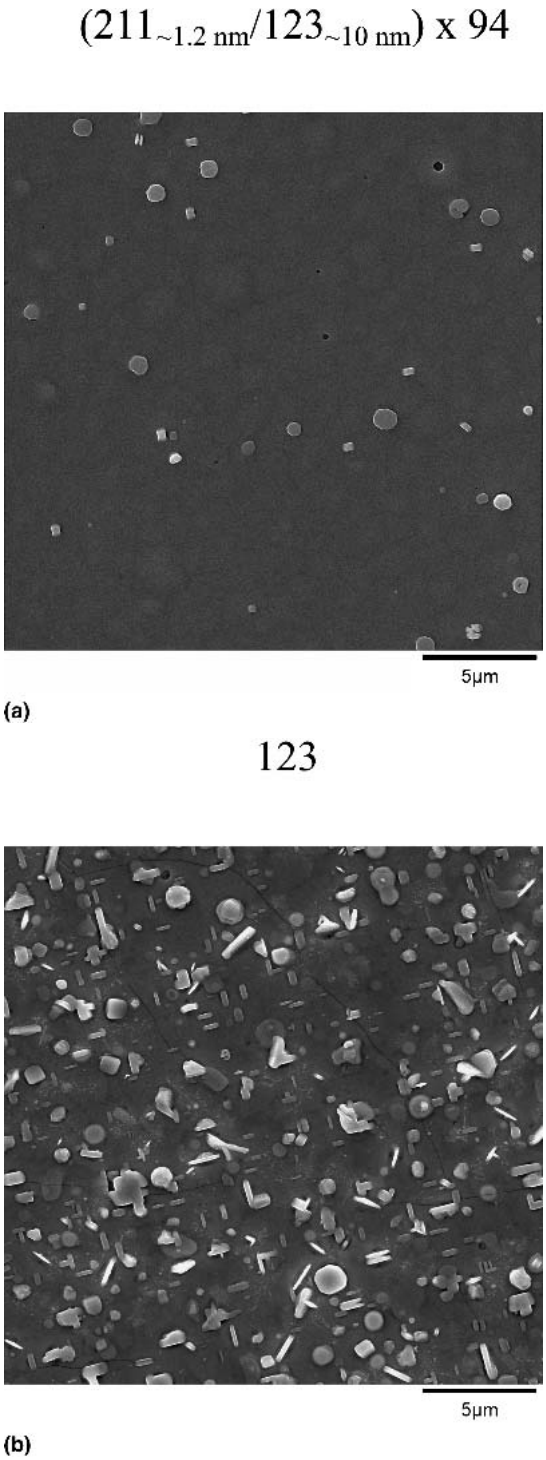

FIG. 5. SEM micrograph of a $(211_{\sim1.2\ nm}/123_{\sim10\ nm})\times94$ multilayer film (top) ~1.0-μm thick compared to a 123 thick film (bottom) with similar thickness.

Finally, we note that the 123 grain size in these conductors has been reduced to about the thickness of the 123 layers of approximately 15 nm, which represents a much smaller dimension for interfilamentary current conduction in Y123 than has been studied thus far. Such

a reduced grain size and the composite nature of the film may also have advantages for coated conductor applications, such as minimizing crack formation during stressing or reducing the effect of damage to any one area.

ACKNOWLEDGMENTS

The Air Force Office of Scientific Research supported this work. The authors would like to thank Dr. R. Wheeler, S. Apt, and L. Piazza of UES Inc. at the Wright-Patterson AFB Materials Directorate for their assistance with SEM and TEM.

REFERENCES

1. A. Bourdillon and N.X. Tan Bourdillon, *High Temperature Superconductors: Processing and Science* (Academic Press, San Diego CA, 1994).
2. D. Larbalestier, A. Gurevich, D. Matthew Feldmann, and A. Polyanskii, Nature **414,** 368 (2001).
3. M. Murakami, D.T. Shaw, and S. Jin, in *Processing and Properties of High T_c Superconductors Volume 1, Bulk Materials*, edited by S. Jin (World Scientific Publishing, River Edge, NJ, 1993).
4. D.C. Larbalestier and M.P. Maley, Mater. Res. Bull. August (1993), p. 50.
5. Y. Iijima, K. Onabe, N. Tugaki, N. Tanabe, N. Sadakara, O. Kohno, and Y. Ikeno, Appl. Phys. Lett. **60,** 769 (1992).
6. X.D. Wu, S.R. Foltyn, P.N. Arendt, W.R. Blumenthal, I.H. Campbell, J.D. Cotton, J.Y. Coulter, W.L. Hults, M.P. Maley, H.F. Safar, and J.L. Smith, Appl. Phys. Lett. **67,** 2397 (1995).
7. A. Goyal, D.P. Norton, J.D. Budai, M. Paranthaman, E.D. Specht, D.M. Kroeger, D.K. Christen, Q. He, B. Saffian, F.A. List, D.F. Lee, P.M. Martin, C.E. Klabunde, E. Hartfield, and V.K. Sikka, Appl. Phys. Lett. **69,** 1795 (1996).
8. S.R. Foltyn, E.J. Peterson, J.Y. Coulter, P.N. Arendt, Q.X. Jia, P.C. Dowden, M.P. Maley, X.D. Wu, and D.E. Peterson, J. Mater. Res. **12,** 2941 (1997).
9. T. Aytug, M. Paranthaman, S. Sathyamurthy, B.W. Kang, D.B. Beach, E.D. Specht, D.F. Lee, R. Feenstra, A. Goyal, D.M. Kroeger, K.J. Leonard, P.M. Martin, and D.K. Christen, *ORNL Superconducting Technology Program for Electric Power Systems,* Annual Report for FY 2001, <http://www.ornl.gov/HTSC/htsc.html>.
10. N. Takezawa and K. Fukushima, Physica C **290,** 31 (1997).
11. *Phase Diagrams for High T_c Superconductors*, edited by J.D. Whitler and R.S. Roth (American Ceramic Society, Westerville OH, 1991).
12. J.M.S. Skakle, Mater. Sci. Eng. **R23,** 1 (1998).
13. K. Reichelt, Vacuum **38**(12), 1083 (1988).
14. V.M. Pan, G.G. Kaminsky, A.L. Kasatkin, M.A. Kuznetsov, V.G. Prokhorov, V.L. Svetchnikov, C.G. Tretiatchenko, V.S. Flis, S.K. Yushchenko, V.I. Matsui, and V.S. Melnikov, Supercond. Sci. Technol. **5,** S48 (1992).
15. M. Murakami, S. Gotoh, H. Fujimoto, K. Yamaguchi, N. Koshizuka, and S. Tanaka, Supercond. Sci. Technol. 4, S43 (1991).
16. S. Jin, G.W. Kamlott, T.H. Tiefel, T. Kodas, T.L. Ward, and D.M. Kroeger, Physica C **181,** 57 (1992).
17. D. Shi, S. Sengupta, J.S. Luo, C. Varanasi, and P.J. McGinn, Physica C **213,** 179 (1993).
18. M. Chopra, S.W. Chan, R.L. Meng, and C.W. Chu, J. Mater. Res. **11,** 1616 (1996).
19. S. Sengupta, D. Shi, J.S. Luo, A. Buzdin, V. Gorin, V.R. Todt, C. Varanasi, and P.J. McGinn, J. Appl. Phys. **81,** 7396 (1997).
20. L. Zhou, S.K. Chen, K.G. Wang, X.Z. Wu, P.X. Zhang, and Y. Feng, Physica C **363,** 99 (2001).
21. T. Haugan, P. Barnes, R. Nekkanti, I. Maartense, L. Brunke, and J. Murphy, in *Extended Abstracts of the 2001 International Workshop on Superconductivity Co-Sponsored by ISTEC and MRS* (ISTEC, Minato-ku, Japan, 2001), p. 111.
22. T.J. Haugan, P.N. Barnes, R.M. Nekkanti, I. Maartense, L.B. Brunke, and J. Murphy in *Materials for High-Temperature Superconductor Technologies*, edited by M.P. Paranthaman, M.W. Rupich, K. Salama, J. Mannhart, and T. Hasegawa (Mater. Res. Soc. Symp. Proc. **689,** Warrendale, PA, 2002), pp. 217–221.
23. J.W. Ekin, T.M. Larson, N.F. Bergren, A.J. Nelson, A.B. Swartzlander, L.L. Kazmerski, A.J. Panson, and B.A. Blankenship, Appl. Phys. Lett. **52,** 1819 (1988).
24. L.F. Goodrich, A.N. Srivastava, T.C. Stauffer, A. Roshko, and L.R. Vale, IEEE Trans Appl. Supercond. **4,** 61 (1994).
25. I. Maartense, A.K. Sarkar, and G. Kozlowski, Physica C **181,** 25 (1991).
26. A. Sarkar, B. Kumar, I. Maartense, and T.L. Peterson, J. Appl. Phys. **65,** 2392 (1989).
27. J.R. Thompson, L. Krusin-Elbaum, Y.C. Kim, D.K. Christen, A.D. Marwick, R. Wheeler, C. Li, S. Patel, D.T. Shaw, P. Lisowski, and J. Ullmann, IEEE Trans. Appl. Supercond. **5,** 1876 (1995).
28. J.R. Thompson, J.G. Ossandon, L. Krusin-Elbaum, H.J. Kim, K.J. Song, D.K. Christen, and J.L. Ullmann, Physica C 378-381 (2002), p. 409.
29. Q.X. Jia, S.R. Foltyn, P.N. Arendt, and J.F. Smith, Appl. Phys. Lett. **80,** 1601 (2002).